Integrated evaluation of aerosols from regional brown hazes over northern China in winter: Concentrations, sources, transformation, and mixing states

Weijun Li,[1,2] Shengzhen Zhou,[1] Xinfeng Wang,[1] Zheng Xu,[1] Chao Yuan,[1] Yangchun Yu,[1] Qingzhu Zhang,[1] and Wenxing Wang[1]

Received 22 September 2010; revised 10 February 2011; accepted 15 February 2011; published 12 May 2011.

[1] To evaluate the wintertime regional brown haze in northern China, trace gases and aerosols were measured at an urban site between 9 and 20 November 2009. Ion chromatography and transmission electron microscopy (TEM) were used to investigate soluble ions in $PM_{2.5}$ and the mixing state of individual particles. The contrasts between clear and hazy days were examined in detail. Concentrations of the primary gases including NO (55.62 ppbv), NO_2 (54.86 ppbv), SO_2 (83.03 ppbv), and CO (2.07 ppmv) on hazy days were 2 to 6 times higher than those on clear days. In contrast, concentrations of O_3 remained low (5.71 ppbv) on hazy days. Mass concentrations of $PM_{2.5}$ (135.90 μg m^{-3}) and BC (7.85 μg m^{-3}) were 3 times higher on hazy days than on clear days. Based on the estimations from TEM analysis, fractions of both ammoniated sulfate (AS)–soot (20%) and AS-soot/organic matter/fly ash (20%) were larger on hazy days than on clear days (13% and 12%), implying that coagulation is an important mixing process in the polluted air. The SO_2 emissions from coal combustion for power plants, industrial activities, and household heating led to high concentrations. Also, high concentrations of secondary sulfates significantly formed in the haze. Therefore, high concentrations of acidic gases contributed to the increased mass and number of secondary aerosols. Our study indicates that metal-catalyzed oxidation in the aqueous phase is a major pathway of sulfate formation. The mixtures of aerosol particles, together with MODIS images, suggest that the hazes covered not only the industrial cities, but extended into the neighboring rural regions.

Citation: Li, W., S. Zhou, X. Wang, Z. Xu, C. Yuan, Y. Yu, Q. Zhang, and W. Wang (2011), Integrated evaluation of aerosols from regional brown hazes over northern China in winter: Concentrations, sources, transformation, and mixing states, *J. Geophys. Res.*, *116*, D09301, doi:10.1029/2010JD015099.

1. Introduction

[2] Atmospheric brown hazes are layers of air pollution consisting of anthropogenic sulfate, nitrate, organics, black carbon (BC), and fly ash, as well as natural aerosols such as sea salt and mineral dust. By scattering and absorbing radiation, aerosol particles of diverse chemical composition have different impacts on the climate system [*Intergovernmental Panel on Climate Change*, 2007]. Brown hazes have far-reaching effects on both regional and global scales [*Quinn and Bates*, 2003], enhancing atmospheric solar heating and decreasing radiation reaching the Earth's surface [*Ramanathan et al.*, 2001; *Seinfeld et al.*, 2004]. Anthropogenic pollutants originating from urban and industrial areas reduce cloud droplet size and suppress precipitation [*Rosenfeld*, 2000]. In particular, absorbing aerosols in hazes play a major role in the regional climate, in the hydrological cycle, and in monsoon rainfall changes [*Menon et al.*, 2002; *Ramanathan and Carmichael*, 2008]. What may be of greater importance, moreover, these aerosol particles cause human health effects such as increased mortality, increased rates of hospital admissions and emergency department visits, exacerbation of chronic respiratory conditions, and decreased lung function, all a consequence of exposure to the air pollution of these persistent hazes [*Hoek et al.*, 2010; *Pope et al.*, 2002].

[3] Some field atmospheric experiments have been conducted to understand the chemical and physical properties of aerosols in regional hazes over different areas such as the Indian Ocean (INDOEX) [*Ramanathan et al.*, 2001] and Mexico City (MILAGRO) [*Querol et al.*, 2008]. These studies revealed that soot particles in haze act as an absorber that warms the atmosphere and cools the Earth's surface [*Ramanathan and Carmichael*, 2008]. However, some of

[1] Environment Research Institute, Shandong University, Jinan, Shandong, China.
[2] State Key Laboratory of Coal Resources and Safe Mining, China University of Mining and Technology, Beijing, China.

Copyright 2011 by the American Geophysical Union.
0148-0227/11/2010JD015099

both the cooling aerosols (e.g., sulfate and nitrate) and the heating aerosols (e.g., soot) do not exist as separate, "externally mixed" particles; rather, an individual aerosol particle can consist of a mixture of cooling and heating aerosols that together form "internally mixed" particles [*Li and Shao*, 2009b; *Pósfai and Buseck*, 2010; *Takahama et al.*, 2010]. Optical effects of such internally mixed aerosols are highly variable and depend on both the region and the season [*Moffet and Prather*, 2009; *Schwarz et al.*, 2008]. Therefore, investigating the mixing state of aerosol particles in regional hazes in different areas and seasons is essential to better understand their effects on regional climate [*Pósfai and Buseck*, 2010].

[4] Over the past few decades regional brown hazes have been a frequent occurrence in northern China. These expansive haze layers sometimes cover six provinces (Shanxi, Hebei, Shandong, Henan, Jiangsu, and Anhui) and two mega cities (Beijing and Tianjin) [*Li and Shao*, 2009b]. Aerosol loadings in northern China are extremely heavy, with a mean aerosol optical depth of 0.5 (increasing to 0.7 in and near major cities) leading to reduced daily mean surface solar radiation of 30 to 40 W m^{-2} [*Li et al.*, 2007b]. As a result, *Chameides et al.* [1999] estimate that regional hazes decrease crop yields by 5 to 30% in China. Moreover, the regional hazes in northern China weaken the seasonal monsoons through their high loading of atmospheric pollutants [*Lau et al.*, 2008]. Although numerous field studies provide abundant information about concentrations, compositions, and optical properties of aerosol particles in urban and background sites in northern China [*Hu et al.*, 2002; *Li et al.*, 2007a; *Pathak et al.*, 2009; *Wang et al.*, 2009], few present data on their actual chemical and physical properties through a combination of single-particle analysis and bulk methods. However, the integrated information not only can elucidate the concentrations and sources of aerosol particles, but can also distinguish primary from secondary aerosols, the latter being produced in chemical reactions involving such gases as SO_2, NO_2, NH_3, and organic gases.

[5] To evaluate the properties of aerosol particles from the brown hazes and to understand haze formation on a regional scale, field measurements were conducted when a strong, northerly cold front from Siberia and Mongolia passed over the whole northern China in November 2009. This frontal passage led to a typical cycle of alternately hazy and clean episodes on a regional scale, a cycle well suited to observe the formation of the regional brown haze with an emphasis on the transports, origins, and mixing mechanisms of aerosol particles. Conducted during 8–20 November 2009, in Jinan city, in the midst of northern China affected by a persistent brown haze layer, this field work determined the mass concentration, size distribution, chemical composition, and mixing state of aerosol particles, as well as concentrations of various trace gases. This field work and subsequent laboratory analyses enabled the comparison of various aerosol particle characteristics among clear, foggy, and hazy days.

2. Experiments

2.1. Measurement Site

[6] Moderate resolution imaging spectroradiometry (MODIS) can reveal and illustrate regional brown hazes, including those over the Yellow Sea (http://modis.gsfc.nasa.gov/). Compared with the MODIS image from the clear day (17 November), the image from the hazy day (20 November) could not clearly display the ground features of the North China Plain or the eastern China coastline because the brown haze layer was too opaque (Figure 1). The regional haze covered nearly all of Anhui, Jiangsu, Henan, Shandong, and southern Hebei provinces, an area of 500,000 km^2. Shandong province lies in the center of this regional brown haze (Figure 1). MODIS satellite images also reveal that huge haze layers are transported across the Shandong peninsula into the Yellow Sea. Jinan city, the capital of Shandong province, turns out to be a geographically representative sampling site for this haze (Figure 1). About 5 km east of downtown, the Jinan atmospheric observatory (N36.68°, E117.06°) is surrounded by densely populated residential areas, urban streets, and light industry. The instruments for this field work were mounted 25 m above ground on the roof of a building on the campus of Shandong University.

2.2. Instruments

[7] Gaseous air pollutants were measured as follows: O_3 by a UV photometric analyzer; CO by a nondispersive infrared analyzer; SO_2 by a pulsed UV fluorescence analyzer; and NO and NO_y by a commercial chemiluminescence analyzer equipped with an external molybdenum oxide (MoO) catalytic converter [*Wang et al.*, 2006]. In addition, $PM_{2.5}$ mass concentrations were measured by a tapered element oscillating microbalance (Thermo Electron Corporation, TEOM 1400a). Mass concentrations of black carbon (BC) were measured by an aethalometer (Magee AE21) with a resolution of 5 min.

[8] Wind direction, wind speed, relative humidity (RH), and temperature were measured and recorded every 5 min. Visibility was estimated at 0800, 1200, and 1700 h every day at the sampling site.

[9] Five cations (Na^+, K^+, NH_4^+, Ca^{2+}, and Mg^{2+}) and five anions (F^-, Cl^-, NO_2^-, NO_3^-, and SO_4^{2-}) in $PM_{2.5}$ were determined by a continuous ambient ion monitor (AIM, URG Corporation, URG9000B), with the system consisting of a particle collection unit and two ion chromatographs (IC) [*Wu and Wang*, 2007].

[10] A wide-range particle spectrometer (WPS™, MSP corporation model 1000XP) continuously measured the number and size distributions of ambient aerosol particles in the range of 10 nm to 10 μm. This instrument is a high-resolution aerosol spectrometer which combines the principles of differential mobility analysis (DMA), condensation particle counting (CPC), and laser light scattering (LPS).

2.3. Aerosol Sampling and Analysis by Transmission Electron Microscopy

[11] Aerosol particles were collected onto copper transmission electron microscopy (TEM) grids coated with carbon film (carbon type-B, 300-mesh copper, Tianld Co., China) by a single-stage cascade impactor with a 0.5-mm-diameter jet nozzle and an airflow rate of 1.0 l min^{-1}. Sampling times varied from 30 s to 5 min, depending on the particle loading as estimated from visibility. Three or four samples were collected around 0900, 1200, and 1800 h each

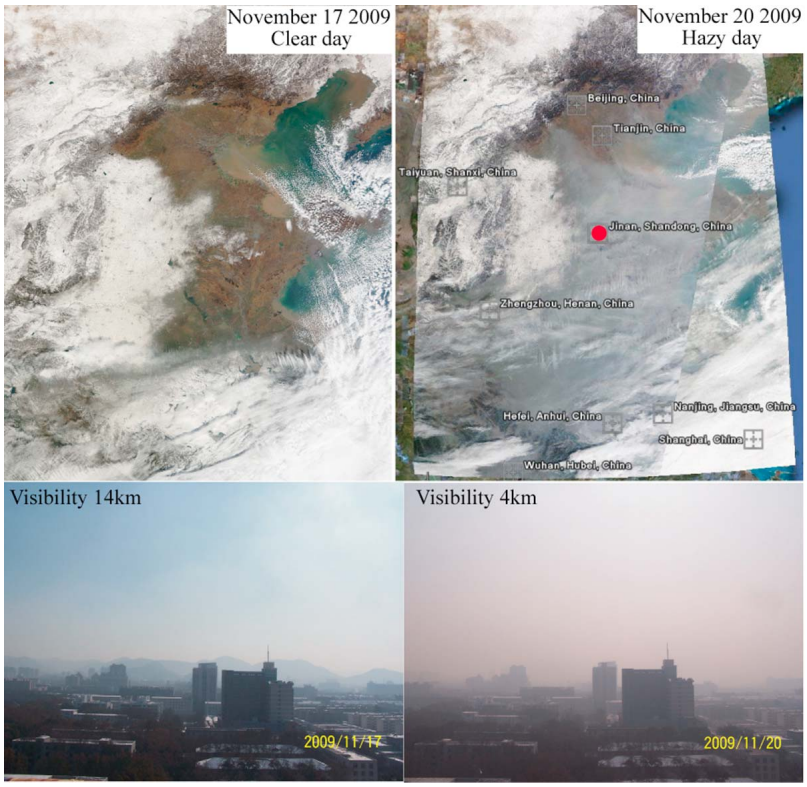

Figure 1. MODIS images and visibility photos taken at sampling site of Jinan. (left) A clear day on 17 November. (right) A haze day on 20 November. White parts in upper two images indicate areas covered with snow or ice. The two photos show visibilities at 14 km on clear day and 4 km on hazy day.

day, with a total of 30 samples between 9 and 20 November 2009. After collection, each sample was placed in a sealed dry plastic tube and stored in a desiccator at 25°C and 20 ± 3% RH to minimize exposure to ambient air and preserve it for analysis. Aerosol particles were analyzed with a JEM-2100 TEM operated at 200 kV. Elemental composition was determined semiquantitatively by using an energy-dispersive X-ray spectrometer (EDS) that can detect elements heavier than C. EDS spectra were collected for 15 s in order to minimize radiation exposure and potential beam damage. Through a labor-intensive operation, hundreds of individual aerosol particles in the samples were only analyzed for size

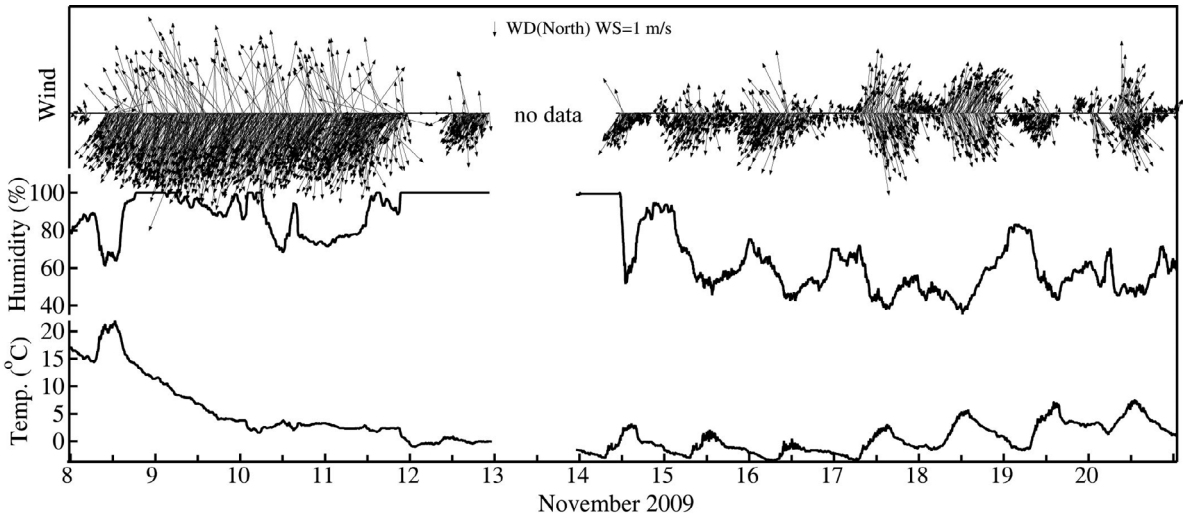

Figure 2. Time series variations of wind direction, wind speed (m s^{-1}), temperature (°C), and relative humidity (%) from 8 to 20 November. No data are available during the snow period.

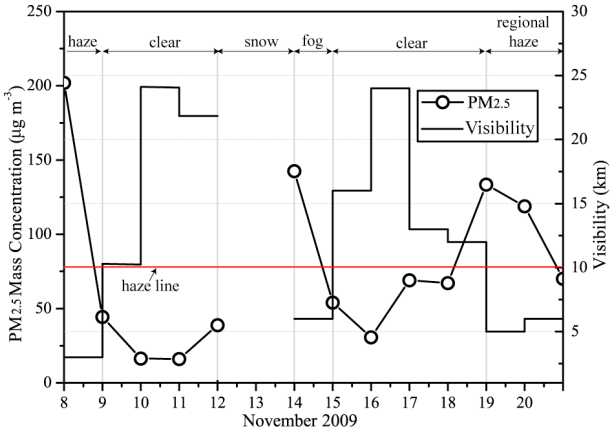

Figure 3. Daily mass concentrations of $PM_{2.5}$ and visibility from 8 to 20 November. Clear, foggy, and hazy days are identified, and no data are available during the snow period. The horizontal line represents a visibility value (10 km) that is used to define the boundary between haze and clear episode.

and elemental composition using TEM/EDS. Therefore, TEM work cannot be good at assessing the contributions of major particles types to these quantities.

2.4. Meteorological Characteristics on Clear, Foggy, and Hazy Days

[12] The Chinese Meteorological Administration (CMA) defines clear, foggy, and hazy days as follows: "clear": visibility ≥ 10 km; "foggy": visibility < 10 km and RH > 90%; "hazy": visibility < 10 km and RH ≤ 80%. All sampling days of the field experiment were categorized with these criteria (Figures 2 and 3).

[13] A strong, northerly cold front from Siberia and Mongolia began to sweep over the North China Plain on 9 November and drastically reduced the ground-level air pollution (Figure 4). This strong synoptic feature lasted 8 days until 16 November. During this period, the wind was from the north with average speeds decreasing from 2.6 m s^{-1} from 9 to 12 November to 0.76 m s^{-1} from 14 to 16 November (Figure 2). According to the CMA report, a snowstorm covered northern China during 12–13 November, and air temperatures were as low as −3°C (Figure 2). This cold weather led to increased household heating throughout northern China.

[14] Although the northwesterly air mass still influenced northern China on 14 November, a severe fog episode occurred in Jinan in that morning (Figure 4). Based on the CMA report, the fog (or mist) occurred in Shandong and southern Hebei provinces after the snowstorm. After the fog episode, clear days returned and lasted from 15 to 18 November.

[15] It should be noted that the prevailing wind direction (Figure 2) and back trajectory of the air mass (Figure 4) changed from north to south at the sampling site on 17 November, indicating that this major synoptic feature had ended. The average wind speed decreased from 0.5 m s^{-1} during 17–18 November to 0.3 m s^{-1} during 19–20 November (Figure 2).

3. Results

3.1. $PM_{2.5}$, BC, and Gaseous Pollutants on Clear, Foggy, and Hazy Days

[16] Variations of $PM_{2.5}$ mass concentration exhibit a strong relationship with wind (Figure 3). The daily $PM_{2.5}$ mass concentration decreased from 202 μg m^{-3} on hazy day (8 November) to 44 μg m^{-3} on clear day (9 November). The lowest daily $PM_{2.5}$ mass concentration (16 μg m^{-3}) of the study period occurred on 11 November (Figure 2). This value is much lower than the average 44 μg m^{-3} measured in winter at the Shangdianzi meteorological station, a regional background site in the North China Plain [*Zhao et al.*, 2009], suggesting that the strong northerly wind (Figure 2) sufficiently swept most anthropogenic air pollutants out of northern China. $PM_{2.5}$ mass concentration on the foggy day (14 November) reached the elevated level of 143 μg m^{-3} (Figure 3). The stable meteorological conditions during the fog episode led to the accumulation of anthropogenic pollutants in urban areas [*Li and Shao*, 2010a]. In addition, following the conversion from clear day (18 November) to hazy day (19 November), daily $PM_{2.5}$ mass concentrations increased from 67 μg m^{-3} to 138 μg m^{-3}.

[17] Summarized in Table 1, daily mass concentrations of $PM_{2.5}$ and BC on foggy and hazy days have similar values

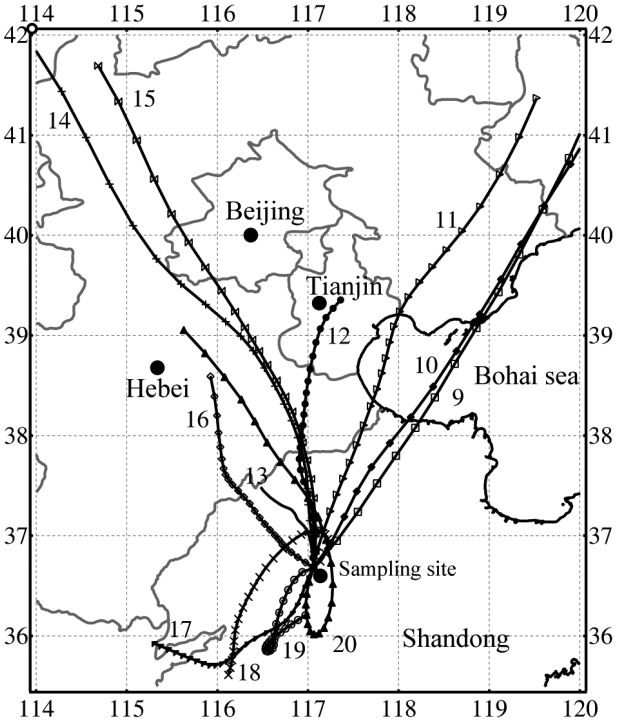

Figure 4. Twelve 24 h air mass back trajectories ending at Jinan from 9 to 20 November. The air masses from 9 to 16 November came from north of Jinan, and others came from south. Markers on the lines denote positions that represent hourly intervals on each back trajectory (http://ready.arl.noaa.gov/HYSPLIT.php).

Table 1. Mixing Ratios of Trace Gases and Mass Concentrations of $PM_{2.5}$ and BC on Clear, Foggy, and Hazy Days

Weather Condition	NO (ppbv)	NO_2 (ppbv)	SO_2 (ppbv)	CO (ppmv)	O_3 (ppbv)	$PM_{2.5}$ ($\mu g\ m^{-3}$)	BC ($\mu g\ m^{-3}$)
Clear	11.26	26.94	34.68	0.79	12.01	45.35	2.81
Foggy	67.40	52.77	80.76	2.59	5.25	142.46	8.30
Hazy	55.62	54.86	83.03	2.07	5.71	135.90	7.85

that are 3 times higher than on clear days. The measured BC concentrations are close to the reported concentrations in Beijing (10 $\mu g\ m^{-3}$) and Shanghai (8 $\mu g\ m^{-3}$), but are much lower than that in Xi'an (20 $\mu g\ m^{-3}$) in winter [*Cao et al.*, 2009; *Yang et al.*, 2005].

[18] Table 1 shows that five gaseous pollutants (e.g., NO, NO_2, O_3, SO_2, and CO) from anthropogenic sources are 2 to 6 times higher on foggy and hazy days than on clear days. *Wang et al.* [2003] reported monthly mixing ratios of 34 ppbv for O_3, 4.4 ppbv for NO, 5.5 ppbv for SO_2, and 0.469 ppmv for CO in November at a rural site in the Pearl River Delta of southern China. Compared to the values found by *Wang et al.* [2003], the average mixing ratios of the trace gases on clear days are still higher in Jinan, even though a strong northwesterly front sufficiently swept out most anthropogenic air pollutants. In contrast, mixing ratios of O_3 remained low (from 5.71 ppbv to 12.01 ppbv), consistent with the reduced photochemical activity expected in winter [*Li et al.*, 2007a].

3.2. Soluble Inorganic Ions in $PM_{2.5}$

[19] Sulfate (SO_4^{2-}), ammonium (NH_4^+), and nitrate (NO_3^-) ions are the major components, together accounting for 53% of $PM_{2.5}$ mass concentration, suggesting that more than half of the aerosol species were formed through atmospheric chemical transformation. Figure 5 shows that the hourly variations of the mass concentrations of those major water-soluble ions in $PM_{2.5}$ display similar patterns. Their highest concentrations occurred on foggy and hazy days; their lowest on clear days, suggesting that the calmer weather of the polluted days, particularly the lower wind speeds, favors the pollutants' transformation and accumulation. *Hu et al.* [2002] also showed that the conversion of acidic gases to aerosol particles depends on meteorological conditions and oxidant concentrations. These major ion concentrations remained at a high level during the fog and hazes (This is discussed in section 4.1).

3.3. Particle Number Concentrations and Size Distributions

[20] Particle number concentrations on clear, foggy, and hazy days are 6,500, 10,400, and 12,400 cm^{-3}, respectively (Figure 6). Their concentration on hazy days is 1.9 times higher than on clear days. The results are consistent with the meteorological observation that the cold fronts from the north transported aerosol particles out of northern China. On the other hand, number-size distributions of aerosol particles on clear, foggy, and hazy days had their highest peaks at 28, 38, and 33, respectively. Figure 6 further shows that three modes including nucleation mode (10–20 nm), Aitken mode (20–100 nm), and accumulation mode (100–1000 nm) on clear, foggy, and hazy days. Particle number has the lowest fraction in the nucleation mode and the highest in the accumulation mode on hazy days, compared with the clear and foggy days. In addition, it is important to note that the number-size distribution of aerosol particles on hazy days had a second, weak peak at 200 nm in the accumulation mode, showing that larger particles can and do occur in the haze (This is described in section 3.4).

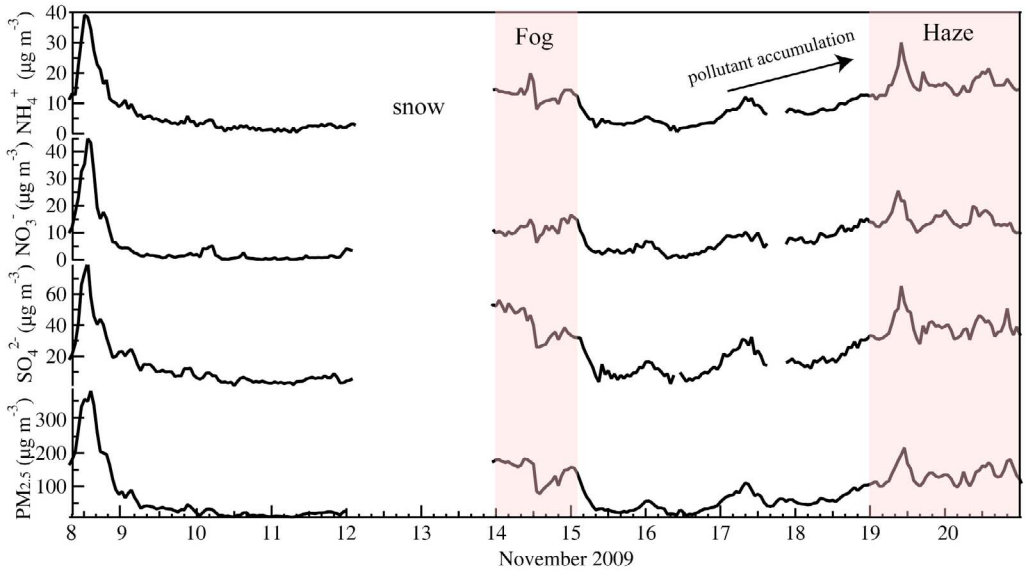

Figure 5. Time series variations of 1 h data for $PM_{2.5}$, SO_4^{2-}, NO_3^-, and NH_4^+ from 8 to 20 November. The high level of mass concentrations of the major ions and $PM_{2.5}$ occurred during the fog and haze episodes.

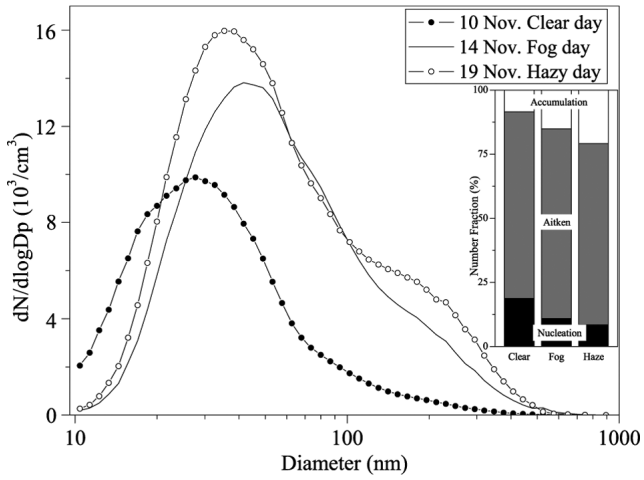

Figure 6. Size distribution and number concentration of aerosol particles on 10 (6,500 cm^{-3} on clear day), 14 (10,400 cm^{-3} on foggy day), and 20 (12,400 cm^{-3} hazy day) November. Nucleation mode (10–20 nm), Aitken mode (20–100 nm), and accumulation mode (100–1000 nm) were separated.

3.4. Particle Classification and Mixing State

[21] On the basis of particle composition and morphology, we classified individual aerosol particles into the following six types: fly ash, organic matter (OM), ammoniated sulfate (AS), soot, mineral particle, and $CaSO_4$ (Figure 7).

[22] Fly ash particles appear as opaque spheres in the TEM images (Figure 7a). EDS spectra show that they mainly contain O, Si, and Al with minor metals (e.g., Fe, Mn, Pb, Ti, and Zn) or O, Fe, Mg, and Zn. Organic aerosols are stable when exposed to a strong electron beam, and they appear as translucent species in TEM images (Figure 7b). They usually contain C and O with minor N and S. The aged OM can be further oxidized to coat inorganic aerosol particles, illustrating that aging changes OM morphology [*Li and Shao*, 2010b; *Moffet et al.*, 2010]. Organic coatings do not exhibit any well-defined shape, and they look like viscous liquids internally mixed in other particles [*Mikhailov et al.*, 2009; *Takahama et al.*, 2010]. Such coatings are difficult to directly identify through particle morphology [*Li and Shao*, 2010b]. In light of this limitation, we focus on the visible OM such as externally mixed OM (Figure 7b) and organic inclusion/aggregations (Figures 8a, 8c, and 8d) in the internally mixed particles. AS particles are a prevalent aerosol component, and consist of O, S, and N with minor Na and K. AS particles are beam sensitive (Figure 7c), mostly leaving S-rich residues and one or more inclusions such as soot, fly ash, and OM, as shown in a previous report by *Li et al.* [2010]. Mineral particles have various irregular shapes (Figure 7d) and most contain Si and Al with Ca, Mg, Fe, Na, and Mn. *Shao et al.* [2008] showed that these natural mineral particles in the atmosphere of northern China mainly consist

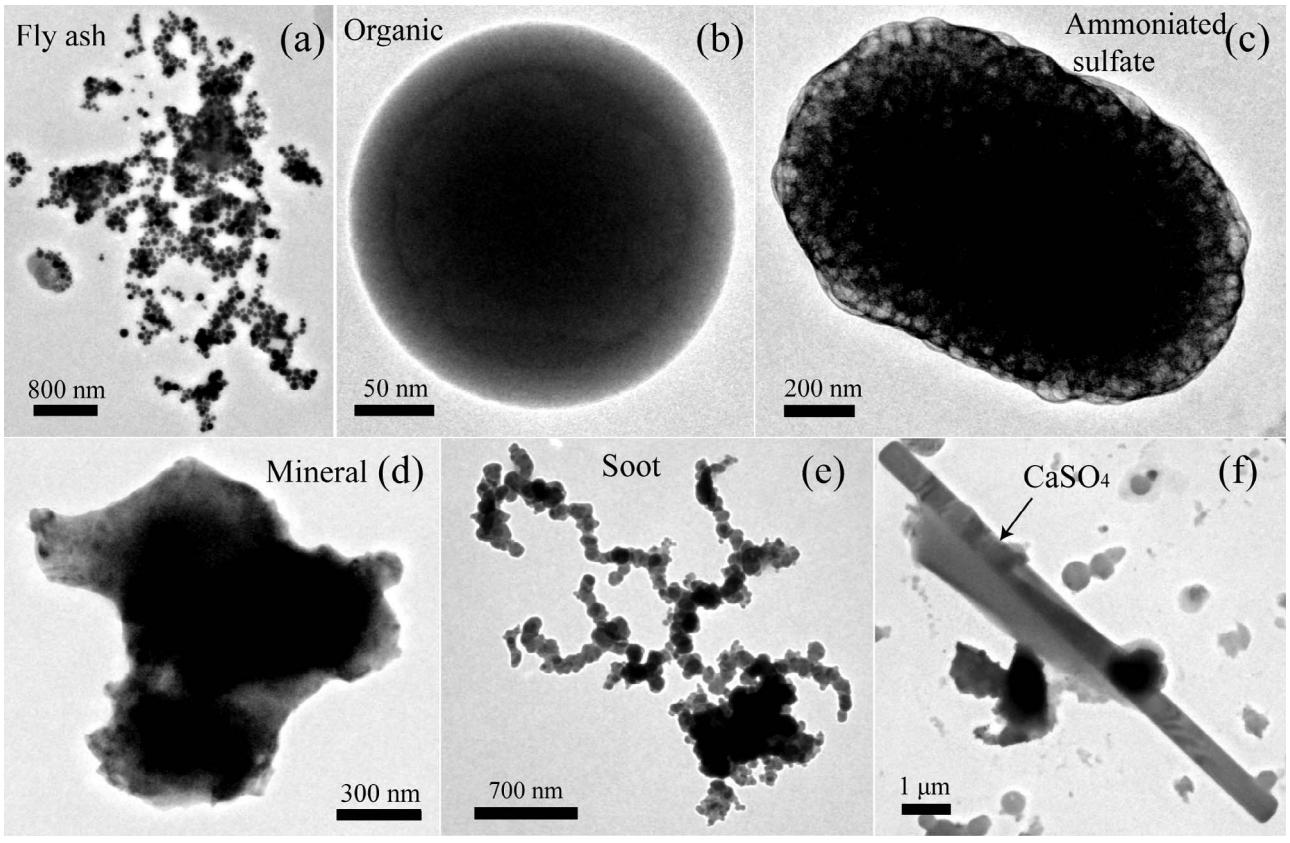

Figure 7. TEM images of (a) fly ash, (b) organic matter (tar ball), (c) ammoniated sulfate, (d) mineral particle, (e) soot, and (f) $CaSO_4$. Compositions of individual aerosol particles were checked using TEM/EDS.

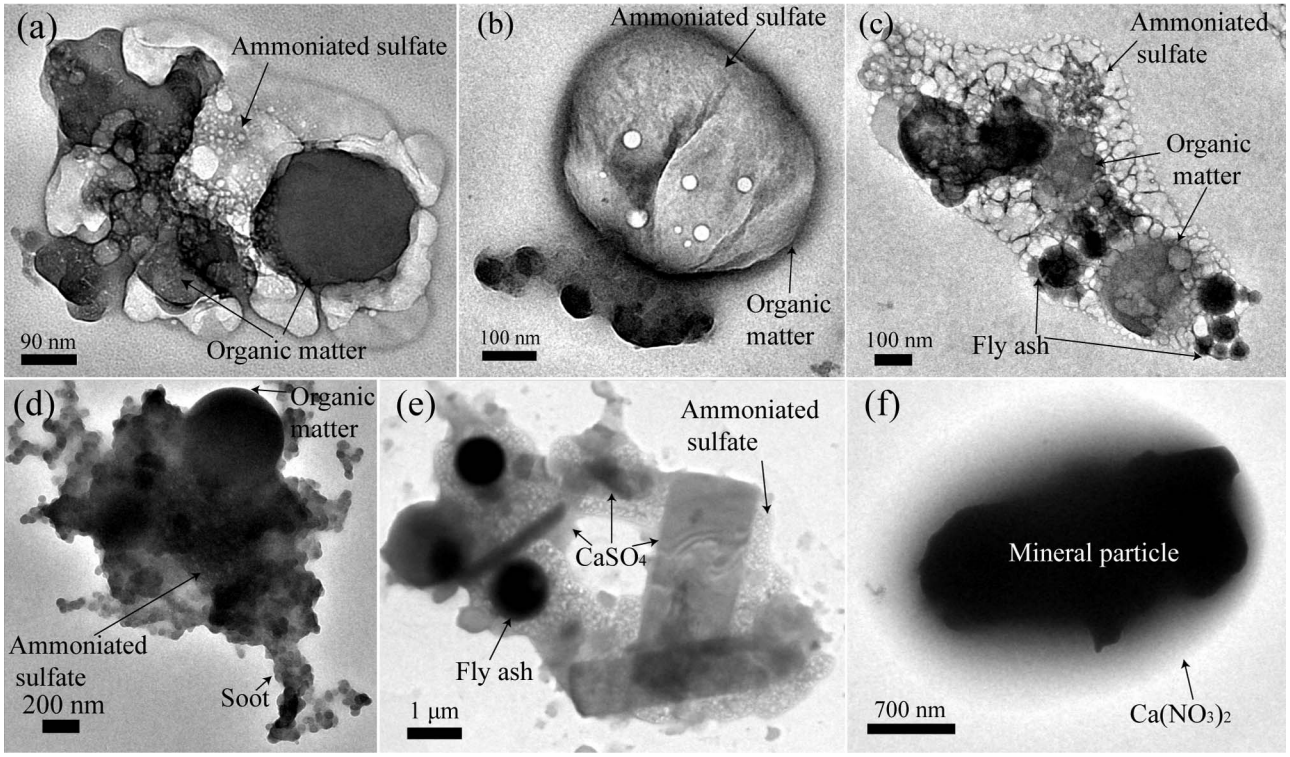

Figure 8. TEM images of the internally mixed particles from hazes. (a) Mixture of ammoniated sulfate and organic particle. (b) Ammoniated sulfate with organic matter. (c) Mixture of ammoniated sulfate, organic matter, and fly ash. (d) Mixture of ammoniated sulfate, organic matter, and soot. (e) Mixture of ammoniated sulfate, $CaSO_4$, and fly ash. (f) Mineral particle coated with $Ca(NO_3)_2$.

of clay, quartz, feldspar, calcite, and dolomite. Soot particles, which contain C with minor O, appear as a chain-like aggregate of carbon-bearing spheres (Figure 7e). The abundant, well-defined $CaSO_4$ particles shown in Figure 7f were found in the samples from hazy days. Overall, based on their different morphology and on certain unique properties under the electron beam, TEM can clearly identify each of the above mentioned particle types.

[23] Numerous studies have shown that aerosol particles from different sources tend to internally mix with each other in the atmosphere as they age. [*Geng et al.*, 2010; *Li and Shao*, 2009b; *Murphy et al.*, 2006; *Pósfai and Buseck*, 2010; *Sullivan et al.*, 2009]. In this study, we also found many different kinds of internally mixed particles (Figure 8), which shows that the fine fly ash, soot, $CaSO_4$, and OM prefer to be inclusions of AS. In addition, some coarse, irregular mineral particles in the haze are coated with $Ca(NO_3)_2$ (Figure 8d), which has been found earlier by *Li and Shao* [2009a].

[24] Based on particle types and mixing states, aerosol particles ranging from 0.01 to 6 μm in diameter are classified into eight classes: AS-soot, AS-OM, AS-fly ash, AS-$CaSO_4$, AS-soot/OM/fly ash, AS-mineral, AS, and others (e.g., soot, fly ash, mineral, OM, or $CaSO_4$).

[25] During the fog, 97% of 348 particles observed are associated with AS. 56% of the particles such as AS-soot, AS-OM, AS-fly ash, and AS-soot/OM/fly ash are internally mixed (Figure 9). 41% of AS and 3% of other particles are externally mixed. On clear days, 86% of 603 particles are associated with AS, and 58% of them are internally mixed. 28% of AS and 14% of other particles are externally mixed. During the haze, 91% of 1,028 particles are associated with AS, and 71% of them are internally mixed. 20% of AS and 9% of other particles are externally mixed. Consistent with

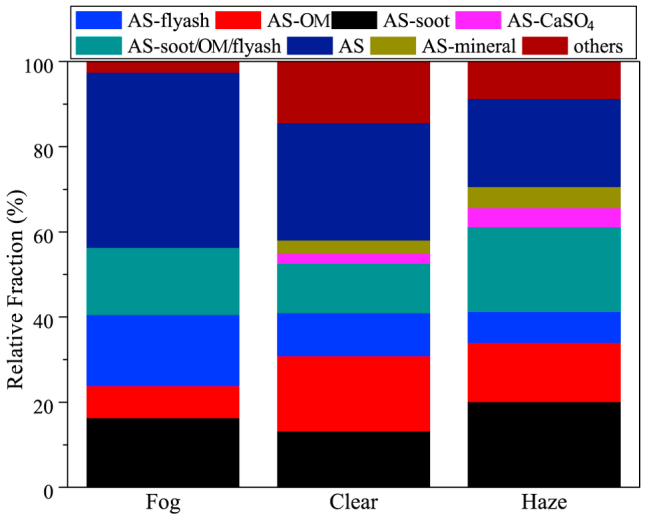

Figure 9. Fractions of different kinds of mixed particles on foggy, clear, and hazy days. AS-soot, AS-OM, AS-fly ash, AS-$CaSO_4$, AS-soot/OM/fly ash, AS, AS-mineral, and others are classified from the TEM observations of individual aerosol particles.

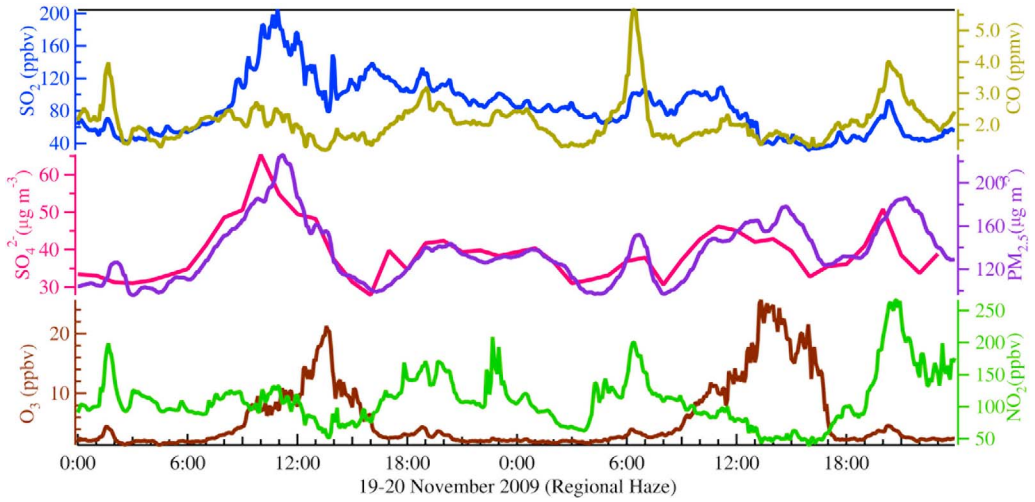

Figure 10. Diurnal concentrations of SO_2, CO, O_3, NO_2, SO_4^{2-}, and $PM_{2.5}$ on hazy days. Concentrations of SO_2, CO, $PM_{2.5}$, O_3, and NO_2 were obtained every 5 min. Concentration of SO_4^{2-} was obtained every hour.

Adachi and Buseck [2010], EDS of AS frequently shows minor metal elements in AS and organic particles, such as Fe, Mn, Ti, Zn, Pb, Hg, and Cd, which are from metal nanoparticles that can become embedded in AS and OM in the atmosphere over industrial areas.

4. Discussion

4.1. Conversions of SO_2 to Particulate Sulfates

[26] During hazy days, diurnal patterns of NO_2 and CO have maxima in the morning and evening rush hours, separated by an afternoon minimum. O_3 had an opposite pattern, with a maximum in the afternoon and minimum in the morning. However, SO_2 exhibited a weak diurnal cycle and remained at high concentrations during hazy days (Figure 10). Based on IC and TEM analysis of aerosol particles, sulfate in $PM_{2.5}$ is a dominant component by mass, with its highest number concentration occurring on hazy days (Figures 5, 6, and 9).

[27] The SO_2 mixing ratio decreased around 1330 h on hazy days but sulfate concentrations increased slightly (Figure 10). The daytime increase of sulfate concentrations has been attributed to the gas-phase oxidation of SO_2 by abundant hydroxyl radical (OH) [*Xiao et al.*, 2009]. Furthermore, *Calvert et al.* [1985] pointed out that H_2O_2 is an important oxidant for the conversion of S(IV) to sulfate in polluted air. However, the rather weak photochemical activity and the high levels of NO_2, as described in section 3.1, result in only a modest production of OH radicals and H_2O_2 [*Hua et al.*, 2008]. Because of the ultralow ozone concentrations, the two proposed mechanisms cannot sufficiently explain the formation of abundant secondary sulfates during the haze episode in winter. In particular, even with the mixing ratio of O_3 at a low level of 3 ppbv, sulfate concentrations are still elevated in the morning and at night (Figure 10).

[28] Recently, *Alexander et al.* [2009] pointed out that sulfates from aqueous SO_2 (S(IV)) oxidation catalyzed by transition metals is an important atmospheric process during winter in the Northern Hemisphere, an alternative to the photochemical pathway that is highly unlikely because of the ultralow O_3 concentrations. Numerous studies have shown that metal catalysis chemistry can promote the conversion of SO_2 to sulfate in fog droplets [*Brandt and Eldik*, 1995; *Calvert et al.*, 1985; *Desboeufs et al.*, 2005; *Reilly et al.*, 2001]. This study confirmed this conversion: TEM analysis found that a large number of fly ash particles (Figure 9) that include transition metals were internally mixed with AS on foggy days, similar to the particles shown in Figures 8c and 8e. The dry aerosol particles on TEM grids collected on foggy day display a conspicuous circle around each and every one (Figure 11a), implying that they have either been in the aqueous phase or have retained water on their surfaces.

[29] The unique morphology of individual aerosol particles was not limited to foggy days, and similar aerosol particles frequently occurred on hazy days, but not on clear days (Figure 11). As a result, many ambient AS particles from hazy days (Figure 11b) should retain considerable water on their surfaces, even though the RH was lower than 80%. *Donaldson and Valsaraj* [2010] showed that these sulfate particles with water film surfaces can enhance oxidation of SO_2. Therefore, transition metal-catalyzed oxidation of S(IV) likely took place on the surface water film or aqueous phase of sulfate particles in the haze (Figure 11b). *Desboeufs et al.* [2005] further showed that aerosols from industrial areas can rapidly release metals that concentrate in the liquid droplets. As a consequence of this release, the metal-bearing AS particles can provide the dissolved metals for the catalyzed oxidation of S(IV) when the surfaces of AS particles become liquid through uptake of water. According to *Alexander et al.* [2009], secondary sulfates formed through transition metal catalysis represent half of the ambient sulfate concentrations in the polluted industrial regions of northern Eurasia. Therefore, in addition to SO_2 oxidation by OH radicals and H_2O_2 in midday, aqueous transition metal-catalyzed oxidation contributes significantly to secondary sulfate formation in wintertime hazes.

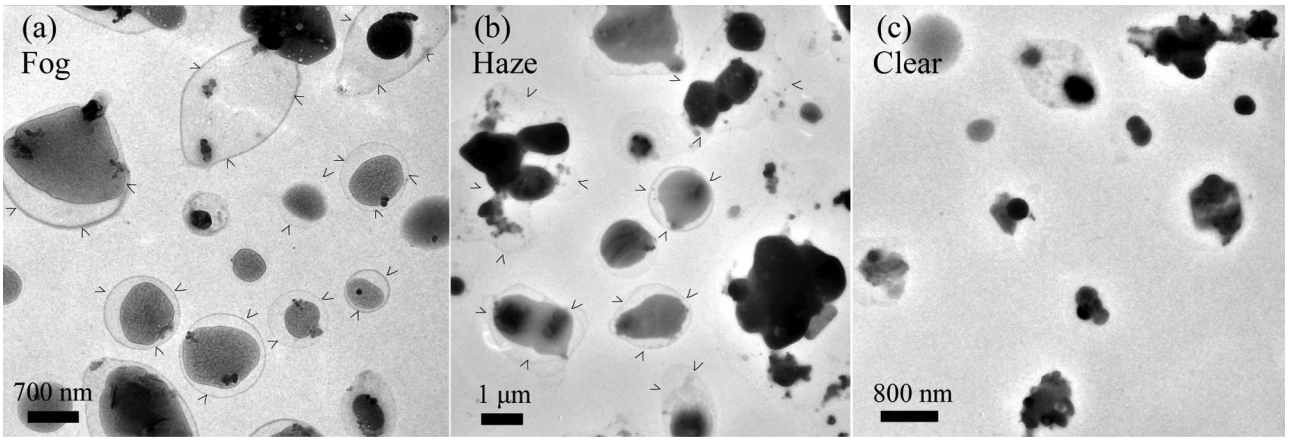

Figure 11. TEM images of aerosol particles from foggy, hazy, and clear days. Three samples were collected around 1000 h on 10 (clear), 14 (fog), and 20 (haze) November, respectively. A conspicuous circle around each particle marked by arrows can be clearly identified in some individual aerosol particles on foggy and hazy days rather than on clear days.

4.2. Sources of the Regional Brown Haze

[30] Compared to the previous study by *Li and Shao* [2009b], a higher number fraction of fly ash particles was encountered, indicating that emissions from coal-fired power plants, industries, and household heating significantly contributed to the brown haze. This conclusion is also supported by the continually high SO_2 concentrations during the haze (Table 1 and Figure 10). Similarly, a continually high CO concentration was also seen on foggy and hazy days (Table 1 and Figure 10). *Li et al.* [2007a] showed that high-efficiency combustion for electricity generation and other industrial activities are likely to be important sources of SO_2 but not CO. In contrast, household heating and cooking in rural areas emit both SO_2 and CO in substantial amounts because of inefficient coal-burning stoves. In rural areas, people often choose cheaper, lower-quality coal for household heating. *Chen et al.* [2006] observed that lower-quality, bituminous coal emits more pollutants (e.g., SO_2, CO, BC, and EC) than anthracite coal. Therefore, emissions from household heating and cooking in rural northern China also significantly contributed to the regional brown haze. In this study, we also noticed that the CO peaks occurred in rush hours (Figure 10). On-road vehicles in urban areas, therefore, are another important source of the haze. As a result, anthropogenic pollutants emitted by fossil fuel (mostly coal) combustion in northern China are the primary cause of the wintertime regional haze, which is exacerbated by light winds (<0.5 m s^{-1}) and stagnant conditions (Figure 2).

4.3. Mixing Mechanisms of Aerosol Particles

[31] To evaluate the transformation and transportation of aerosol particles in different atmospheric environments, the mixing states of individual aerosol particles should be investigated [*Li and Shao*, 2009a; *Pósfai and Buseck*, 2010; *Zhang et al.*, 2000]. Moreover, knowledge of mixing states is important to estimate the optical properties of aerosol particles in the troposphere [*Lang-Yona et al.*, 2010; *Moffet and Prather*, 2009; *Schwarz et al.*, 2008; *Takahama et al.*, 2010]. Our analysis demonstrates that AS aerosols in the haze were broadly internally mixed with refractory aerosol particles such as soot, fly ash, mineral, $CaSO_4$, and OM (Figure 8). In particular, some AS particles had two or more inclusions. Even though similarly internally mixed aerosol classes occurred on clear and hazy days, they displayed different fractions (Figure 9). Relative number fractions of both AS-soot (20%) and AS-soot/OM/fly ash (20%) from hazy days exceed those (13% and 12%) of clear days, implying that coagulation of aerosol particles was more significant in the polluted air. In agreement, Figure 6 shows low number fractions in the nucleation mode and high fractions in the Aitken and accumulation mode on hazy days. *Wu et al.* [2007] found that high concentrations of preexisting aerosol particles in the polluted air of northern China suppressed new particle formation in nucleation mode but enhanced aerosol coagulation. In addition, the gas-to-particulate mass conversion for particle growth, which takes place as condensation in the aqueous phase, was also an important process in the polluted air of northern China [*Wehner et al.*, 2008]. The chemical conversion of SO_2 to particulate sulfates in haze probably took place on the surface water-film of the aerosol particles, as noted in section 4.1. This conclusion partly explains why most AS particles occur in the Aitken mode. Therefore, the mean diameter of aerosol particles is slightly larger on hazy days than on clear days, probably because the aging by condensation and coagulation of hazy days exceeded that of clear days. This result agrees well with the size distributions of aerosol particles on hazy and clear days shown in Figure 6.

[32] TEM observations estimated that 71% of aerosol particles on hazy days are internally mixed (Figure 9). This value is higher than the 56% on foggy days and the 58% on clear days, suggesting that sulfate particles in the haze were aged longer. These internally mixed aerosol particles can exhibit different optical and hygroscopic properties than the original particles [*Moffet and Prather*, 2009; *Pan et al.*, 2009; *Zhang et al.*, 2008]. When these aged aerosol particles are entrained and transported, they can act as CCN. In particular, the copious AS-soot and AS-soot/OM/fly ash particles from the regional haze directly and indirectly enhance its overall scattering and absorption [*Lang-Yona*

et al., 2010; *Schwarz et al.*, 2008]. These aged particles in the haze layer probably increase upper atmospheric heating and at the same time cool the ground [*Ramanathan and Carmichael*, 2008]. The decrease of solar radiation in the North China Plain can reduce the yields of the all-important winter wheat crop. Once aerosols alter the radiation budgets of the lower and upper atmospheres, haze episodes may persist because of the enhanced atmospheric stability. On the other hand, these fine particulates, particularly those internally mixed with metal or metal-bearing particles, can cause many of the more deleterious health effects.

5. Conclusions

[33] Aerosol particles were collected between 9 and 20 November 2009, in Jinan city. Clear, foggy, and hazy days were classified according to their visibility and RH. MODIS images showed that the regional haze covered Anhui, Jiangsu, Henan, Shandong, and the south part of Hebei province, an area of 500,000 km^2.

[34] Mixing ratios of trace gases (i.e., NO, NO_2, SO_2, and CO) from anthropogenic sources were 2 to 6 times higher on foggy and hazy days than on clear days. O_3 concentrations remained at low levels throughout the study. Daily mean concentrations of $PM_{2.5}$ and BC on foggy and hazy days had similar values, 3 times higher than on clear days. Sulfate, ammonium, and nitrate ions are major aerosol components, accounting for 53% of $PM_{2.5}$ mass concentrations. The number concentrations of aerosol particles (10 nm to 10 μm) on hazy days were 12,400 cm^{-3}, nearly twice those on clear days.

[35] The different composition and morphology of individual aerosol particles led to their classification into the following six types: fly ash, OM, AS, soot, mineral particle, and $CaSO_4$. Based on their mixing states, aerosol particles were further grouped into eight classes: AS-soot, AS-OM, AS-fly ash, AS-$CaSO_4$, AS-soot/OM/fly ash, AS, AS-mineral, and others. Based on the estimations from TEM analysis, relative number fractions of both AS-soot (20%) and AS-soot/OM/fly ash (20%) from hazy days exceeded those of clear days ((13% and 12%), implying that coagulation is an important mixing mechanism in polluted air.

[36] SO_2 exhibited a weak diurnal cycle with persistently high concentrations during the haze, suggesting that SO_2 emissions from power plant and industrial coal combustion, residential and commercial heating, and cooking in northern China were principle contributors. Based on IC and TEM analysis of aerosol particles from hazy days, sulfates dominated in both mass and number. In addition to the SO_2 partly oxidized by OH radicals and H_2O_2, aqueous transition metal-catalyzed oxidation by O_2 on the surfaces of pre-existing sulfate particles significantly transformed SO_2 into particulate sulfates. Therefore, the rapid conversion of SO_2 to sulfates not only enhanced their distribution in the Aitken mode but also induced these sulfates to increase their sizes by condensation.

[37] Overall, we conclude that anthropogenic pollutants emitted by fossil fuel (mostly coal) combustion in northern China led to the formation of the widespread, wintertime, regional haze, itself exacerbated by light winds (<0.5 m s^{-1}) associated with enhanced boundary layer stability.

[38] **Acknowledgments.** We appreciate Peter Hyde's comments and proofreading. Financial supports were provided by National Basic Research Program of China (2005CB422203 and 2011CB403401), State Key Laboratory of Coal Resources and Safe Mining (SKLCRSM09KFB04), China Postdoctoral Science Foundation funded project (20090461213 and 201003635), Independent Innovation Foundation of Shandong University, and Shandong Postdoctoral Science Innovation Foundation (200902016).

References

Adachi, K., and P. R. Buseck (2010), Hosted and free-floating metal-bearing atmospheric nanoparticles in Mexico City, *Environ. Sci. Technol.*, *44*(7), 2299–2304, doi:10.1021/es902505b.

Alexander, B., R. J. Park, D. J. Jacob, and S. Gong (2009), Transition metal-catalyzed oxidation of atmospheric sulfur: Global implications for the sulfur budget, *J. Geophys. Res.*, *114*, D02309, doi:10.1029/2008JD010486.

Brandt, C., and R. V. Eldik (1995), Transition metal-catalyzed oxidation of sulfur(IV) oxides. Atmospheric-relevant processes and mechanisms, *Chem. Rev.*, *95*(1), 119–190, doi:10.1021/cr00033a006.

Calvert, J., A. Lazrus, G. Kok, B. Heikes, J. Walega, J. Lind, and C. Cantrell (1985), Chemical mechanisms of acid generation in the troposphere, *Nature*, *317*, 27–35, doi:10.1038/317027a0.

Cao, J.-J., C.-S. Zhu, J. C. Chow, J. G. Watson, Y.-M. Han, G.-h. Wang, Z.-x. Shen, and Z.-S. An (2009), Black carbon relationships with emissions and meteorology in Xi'an, China, *Atmos. Res.*, *94*(2), 194–202, doi:10.1016/j.atmosres.2009.05.009.

Chameides, W. L., et al. (1999), Case study of the effects of atmospheric aerosols and regional haze on agriculture: An opportunity to enhance crop yields in China through emission controls?, *Proc. Natl. Acad. Sci. U. S. A.*, *96*(24), 13,626–13,633, doi:10.1073/pnas.96.24.13626.

Chen, Y., G. Zhi, Y. Feng, J. Fu, J. Feng, G. Sheng, and B. R. T. Simoneit (2006), Measurements of emission factors for primary carbonaceous particles from residential raw-coal combustion in China, *Geophys. Res. Lett.*, *33*, L20815, doi:10.1029/2006GL026966.

Desboeufs, K. V., A. Sofikitis, R. Losno, J. L. Colin, and P. Ausset (2005), Dissolution and solubility of trace metals from natural and anthropogenic aerosol particulate matter, *Chemosphere*, *58*(2), 195–203, doi:10.1016/j.chemosphere.2004.02.025.

Donaldson, D. J., and K. T. Valsaraj (2010), Adsorption and reaction of trace gas-phase organic compounds on atmospheric water film surfaces, *Crit. Rev. Environ. Sci. Technol.*, *44*(3), 865–873.

Geng, H., S. Kang, H.-J. Jung, M. Choel, H. Kim, and C.-U. Ro (2010), Characterization of individual submicrometer aerosol particles collected in Incheon, Korea, by quantitative transmission electron microscopy energy-dispersive X-ray spectrometry, *J. Geophys. Res.*, *115*, D15306, doi:10.1029/2009JD013486.

Hoek, G., et al. (2010), Concentration response functions for ultrafine particles and all-cause mortality and hospital admissions: Results of a European Expert panel elicitation, *Environ. Sci. Technol.*, *44*(1), 476–482, doi:10.1021/es9021393.

Hu, M., L. Y. He, Y. H. Zhang, M. Wang, Y. P. Kim, and K. C. Moon (2002), Seasonal variation of ionic species in fine particles at Qingdao, China, *Atmos. Environ.*, *36*(38), 5853–5859, doi:10.1016/S1352-2310(02)00581-2.

Hua, W., et al. (2008), Atmospheric hydrogen peroxide and organic hydroperoxides during PRIDE-PRD'06, China: Their concentration, formation mechanism and contribution to secondary aerosols, *Atmos. Chem. Phys.*, *8*(22), 6755–6773, doi:10.5194/acp-8-6755-2008.

Intergovernmental Panel on Climate Change (2007), *Climate Change 2007: The Physical Science Basis. Contribution of Working Group I to the Fourth Assessment Report of the Intergovernmental Panel on Climate Change*, edited by S. Solomon et al., 1056 pp., IPCC, Cambridge, U. K.

Lang-Yona, N., A. Abo-Riziq, C. Erlick, E. Segre, M. Trainic, and Y. Rudich (2010), Interaction of internally mixed aerosols with light, *Phys. Chem. Chem. Phys.*, *12*(1), 21–31, doi:10.1039/b913176k.

Lau, K. M., et al. (2008), The Joint Aerosol-Monsoon Experiment: A new challenge for monsoon climate research, *Bull. Am. Meterorol. Soc.*, *89*(3), 369–383, doi:10.1175/BAMS-89-3-369.

Li, C., L. T. Marufu, R. R. Dickerson, Z. Li, T. Wen, Y. Wang, P. Wang, H. Chen, and J. W. Stehr (2007a), In situ measurements of trace gases and aerosol optical properties at a rural site in northern China during East Asian Study of Tropospheric Aerosols: An International Regional Experiment 2005, *J. Geophys. Res.*, *112*, D22S04, doi:10.1029/2006JD007592.

Li, W. J., and L. Y. Shao (2009a), Observation of nitrate coatings on atmospheric mineral dust particles, *Atmos. Chem. Phys.*, *9*(6), 1863–1871, doi:10.5194/acp-9-1863-2009.

Li, W. J., and L. Y. Shao (2009b), Transmission electron microscopy study of aerosol particles from the brown hazes in northern China, *J. Geophys. Res.*, *114*, D09302, doi:10.1029/2008JD011285.

Li, W. J., and L. Y. Shao (2010a), Characterization of mineral particles in winter fog of Beijing analyzed by TEM and SEM, *Environ. Monit. Assess.*, *161*(1), 565–573, doi:10.1007/s10661-009-0768-1.

Li, W. J., and L. Y. Shao (2010b), Mixing and water-soluble characteristics of particulate organic compounds in individual urban aerosol particles, *J. Geophys. Res.*, *115*, D02301, doi:10.1029/2009JD012575.

Li, W. J., L. Y. Shao, and P. R. Buseck (2010), Haze types in Beijing and the influence of agricultural biomass burning, *Atmos. Chem. Phys.*, *10*(17), 8119–8130, doi:10.5194/acp-10-8119-2010.

Li, Z. Q., et al.. (2007b), Aerosol optical properties and their radiative effects in northern China, *J. Geophys. Res.*, *112*, D22S01, doi:10.1029/2006JD007382.

Menon, S., J. Hansen, L. Nazarenko, and Y. F. Luo (2002), Climate effects of black carbon aerosols in China and India, *Science*, *297*(5590), 2250–2253, doi:10.1126/science.1075159.

Mikhailov, E., S. Vlasenko, S. T. Martin, T. Koop, and U. Poschl (2009), Amorphous and crystalline aerosol particles interacting with water vapor: Conceptual framework and experimental evidence for restructuring, phase transitions and kinetic limitations, *Atmos. Chem. Phys.*, *9*(24), 9491–9522, doi:10.5194/acp-9-9491-2009.

Moffet, R. C., and K. A. Prather (2009), In-situ measurements of the mixing state and optical properties of soot with implications for radiative forcing estimates, *Proc. Natl. Acad. Sci. U. S. A.*, *106*(29), 11,872–11,877, doi:10.1073/pnas.0900040106.

Moffet, R. C., et al. (2010), Microscopic characterization of carbonaceous aerosol particle aging in the outflow from Mexico City, *Atmos. Chem. Phys.*, *10*(3), 961–976, doi:10.5194/acp-10-961-2010.

Murphy, D. M., D. J. Cziczo, K. D. Froyd, P. K. Hudson, B. M. Matthew, A. M. Middlebrook, R. E. Peltier, A. Sullivan, D. S. Thomson, and R. J. Weber (2006), Single-particle mass spectrometry of tropospheric aerosol particles, *J. Geophys. Res.*, *111*, D23S32, doi:10.1029/2006JD007340.

Pan, X. L., P. Yan, J. Tang, J. Z. Ma, Z. F. Wang, A. Gbaguidi, and Y. L. Sun (2009), Observational study of influence of aerosol hygroscopic growth on scattering coefficient over rural area near Beijing mega-city, *Atmos. Chem. Phys.*, *9*(19), 7519–7530, doi:10.5194/acp-9-7519-2009.

Pathak, R. K., W. S. Wu, and T. Wang (2009), Summertime PM2.5 ionic species in four major cities of China: Nitrate formation in an ammonia-deficient atmosphere, *Atmos. Chem. Phys.*, *9*(5), 1711–1722, doi:10.5194/acp-9-1711-2009.

Pope, C. A., R. T. Burnett, M. J. Thun, E. E. Calle, D. Krewski, K. Ito, and G. D. Thurston (2002), Lung cancer, cardiopulmonary mortality, and long-term exposure to fine particulate air pollution, *J. Am. Med. Assoc.*, *287*(9), 1132–1141, doi:10.1001/jama.287.9.1132.

Pósfai, M., and P. R. Buseck (2010), Nature and climate effects of individual tropospheric aerosol particles, *Annu. Rev. Earth Planet. Sci.*, *38*(1), 17–43, doi:10.1146/annurev.earth.031208.100032.

Querol, X., et al. (2008), PM speciation and sources in Mexico during the MILAGRO-2006 campaign, *Atmos. Chem. Phys.*, *8*(1), 111–128, doi:10.5194/acp-8-111-2008.

Quinn, P. K., and T. S. Bates (2003), North American, Asian, and Indian haze: Similar regional impacts on climate?, *Geophys. Res. Lett.*, *30*(11), 1555, doi:10.1029/2003GL016934.

Ramanathan, V., and G. Carmichael (2008), Global and regional climate changes due to black carbon, *Nat. Geosci.*, *1*(4), 221–227, doi:10.1038/ngeo156.

Ramanathan, V., et al. (2001), Indian Ocean experiment: An integrated analysis of the climate forcing and effects of the great Indo-Asian haze, *J. Geophys. Res.*, *106*(D22), 28,371–28,398, doi:10.1029/2001JD900133.

Reilly, J. E., O. V. Rattigan, K. F. Moore, C. Judd, D. Eli Sherman, V. A. Dutkiewicz, S. M. Kreidenweis, L. Husain, and J. L. Collett (2001), Drop size-dependent S(IV) oxidation in chemically heterogeneous radiation fogs, *Atmos. Environ.*, *35*(33), 5717–5728, doi:10.1016/S1352-2310(01)00373-9.

Rosenfeld, D. (2000), Suppression of rain and snow by urban and industrial air pollution, *Science*, *287*(5459), 1793–1796, doi:10.1126/science.287.5459.1793.

Schwarz, J. P., et al. (2008), Coatings and their enhancement of black carbon light absorption in the tropical atmosphere, *J. Geophys. Res.*, *113*, D03203, doi:10.1029/2007JD009042.

Seinfeld, J. H., et al. (2004), ACE-ASIA: Regional climatic and atmospheric chemical effects of Asian dust and pollution, *Bull. Am. Meterorol. Soc.*, *85*(3), 367–380, doi:10.1175/BAMS-85-3-367.

Shao, L. Y., W. J. Li, Z. H. Xiao, and Z. Q. Sun (2008), The mineralogy and possible sources of spring dust particles over Beijing, *Adv. Atmos. Sci.*, *25*(3), 395–403, doi:10.1007/s00376-008-0395-8.

Sullivan, R. C., M. J. K. Moore, M. D. Petters, S. M. Kreidenweis, G. C. Roberts, and K. A. Prather (2009), Effect of chemical mixing state on the hygroscopicity and cloud nucleation properties of calcium mineral dust particles, *Atmos. Chem. Phys.*, *9*(10), 3303–3316, doi:10.5194/acp-9-3303-2009.

Takahama, S., S. Liu, and L. M. Russell (2010), Coatings and clusters of carboxylic acids in carbon-containing atmospheric particles from spectromicroscopy and their implications for cloud-nucleating and optical properties, *J. Geophys. Res.*, *115*, D01202, doi:10.1029/2009JD012622.

Wang, T., C. N. Poon, Y. H. Kwok, and Y. S. Li (2003), Characterizing the temporal variability and emission patterns of pollution plumes in the Pearl River Delta of China, *Atmos. Environ.*, *37*(25), 3539–3550, doi:10.1016/S1352-2310(03)00363-7.

Wang, T., H. L. A. Wong, J. Tang, A. Ding, W. S. Wu, and X. C. Zhang (2006), On the origin of surface ozone and reactive nitrogen observed at a remote mountain site in the northeastern Qinghai-Tibetan Plateau, western China, *J. Geophys. Res.*, *111*, D08303, doi:10.1029/2005JD006527.

Wang, Y., H. Che, J. Ma, Q. Wang, G. Shi, H. Chen, P. Goloub, and X. Hao (2009), Aerosol radiative forcing under clear, hazy, foggy, and dusty weather conditions over Beijing, China, *Geophys. Res. Lett.*, *36*, L06804, doi:10.1029/2009GL037181.

Wehner, B., W. Birmili, F. Ditas, Z. Wu, M. Hu, X. Liu, J. Mao, N. Sugimoto, and A. Wiedensohler (2008), Relationships between submicrometer particulate air pollution and air mass history in Beijing, China, 2004–2006, *Atmos. Chem. Phys.*, *8*(20), 6155–6168, doi:10.5194/acp-8-6155-2008.

Wu, W. S., and T. Wang (2007), On the performance of a semi-continuous PM2.5 sulphate and nitrate instrument under high loadings of particulate and sulphur dioxide, *Atmos. Environ.*, *41*(26), 5442–5451, doi:10.1016/j.atmosenv.2007.02.025.

Wu, Z., M. Hu, S. Liu, B. Wehner, S. Bauer, A. Ma ßling, A. Wiedensohler, T. Petäjä, M. Dal Maso, and M. Kulmala (2007), New particle formation in Beijing, China: Statistical analysis of a 1-year data set, *J. Geophys. Res.*, *112*, D09209, doi:10.1029/2006JD007406.

Xiao, R., et al. (2009), Formation of submicron sulfate and organic aerosols in the outflow from the urban region of the Pearl River Delta in China, *Atmos. Environ.*, *43*(24), 3754–3763, doi:10.1016/j.atmosenv.2009.04.028.

Yang, F., K. He, B. Ye, X. Chen, L. Cha, S. H. Cadle, T. Chan, and P. A. Mulawa (2005), One-year record of organic and elemental carbon in fine particles in downtown Beijing and Shanghai, *Atmos. Chem. Phys.*, *5*, 1449–1457, doi:10.5194/acp-5-1449-2005.

Zhang, D. Z., G. Y. Shi, Y. Iwasaka, and M. Hu (2000), Mixture of sulfate and nitrate in coastal atmospheric aerosols: Individual particle studies in Qingdao (36°04′N, 120°21′E), China, *Atmos. Environ.*, *34*(17), 2669–2679, doi:10.1016/S1352-2310(00)00078-9.

Zhang, R. Y., A. F. Khalizov, J. Pagels, D. Zhang, H. X. Xue, and P. H. McMurry (2008), Variability in morphology, hygroscopicity, and optical properties of soot aerosols during atmospheric processing, *Proc. Natl. Acad. Sci. U. S. A.*, *105*(30), 10,291–10,296, doi:10.1073/pnas.0804860105.

Zhao, X., X. Zhang, X. Xu, J. Xu, W. Meng, and W. Pu (2009), Seasonal and diurnal variations of ambient PM2.5 concentration in urban and rural environments in Beijing, *Atmos. Environ.*, *43*(18), 2893–2900, doi:10.1016/j.atmosenv.2009.03.009.

W. Li, W. Wang, X. Wang, Z. Xu, Y. Yu, C. Yuan, Q. Zhang, and S. Zhou, Environment Research Institute, Shandong University, Jinan, Shandong 250100, China. (liweijun@sdu.edu.cn; wxwang@sdu.edu.cn)